Topology-induced symmetry breaking: a demonstration in antiferromagnetic magnons on a Möbius strip

Kuangyin Deng[1,*] and Ran Cheng[1,2,†]

[1] *Department of Electrical and Computer Engineering, University of California, Riverside, California 92521, USA*

[2] *Department of Physics and Astronomy, University of California, Riverside, California 92521, USA*

We propose a mechanism of topology-induced symmetry breaking, where certain local symmetry preserved by the Hamiltonian is broken in the excited eigenstates due to the nontrivial boundary condition. As a demonstration, we study magnon excitations on a Möbius strip comprising of two antiferromagnetically coupled spin chains. Even under a simple Hamiltonian respecting local rotational symmetry and without considering curvature effects, magnons exhibit linear polarization of the Néel vector devoid of chirality and form two non-degenerate branches that cannot be smoothly connected to or be decomposed by the circularly-polarized magnons typically seen in antiferromagnets. One branch supports standing-wave formation on the Möbius strip while the other does not, owing to its spectral shift incurred by the boundary condition. Our findings showcase the significant influence of real-space topology on the physical nature of quasiparticles.

Introduction. In solid-state systems, physical properties of quasiparticles are believed to be direct manifestations of symmetry and interactions, whereas the subtle impact of real-space topology remains elusive. Prevailing studies often adopt periodic boundary conditions (PBCs) on the quasiparticles [1], for which the system becomes topologically equivalent to a circle, a torus, or a 3D-torus depending on the dimensionality. However, there exist exotic structures such as Möbius strips and Klein bottles that do not conform with the PBCs. Concerning the physical behavior of quasiparticles on such an object, it is tempting to ask: what are the physical implications of the non-trivial boundary conditions?

By topological nature, a Möbius strip is non-orientable with a single surface and a single edge, hence precluding the application of any ordinary PBC. Recently, elementary excitations residing on Möbius strips have aroused increasing theoretical attentions [2–9]. Experimentally, Möbius strips have been realized in a wide range of systems such as molecules [10, 11], single crystals [12], resonators [13–15], and optical cavities [16, 17], fertilizing a vibrant arena for exploring new physics emerging from the Möbius topology. However, most of these studies focused on the local curvature effects of the strip based on continuous geometry. It is far from clear if there are any residual consequences arising *only* from the Möbius boundary condition when spatial curvature is discarded.

In this Letter, we propose a hitherto unknown mechanism, dubbed *topology-induced symmetry breaking* (TISB), which unravels the extraordinary behavior of quasiparticles enabled exclusively by the topological boundary conditions (TBCs) but has nothing to do with any curvature effects. TISB refers to a situation that certain local symmetry respected by the Hamiltonian is explicitly broken in the eigenspace of quasiparticles. While this new mechanism could entail profound consequences in various systems with non-trivial real-space topology, here we demonstrate its manifestation in magnonic excitations on a Möbius strip.

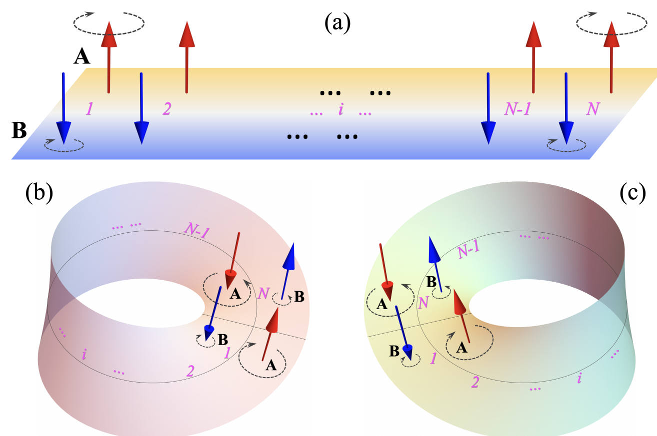

FIG. 1. Schematic illustration of the system. (a) An AFM nano-ribbon consists of two ferromagnetic spin chains, where the red (blue) arrows signify the equilibrium spin orientation of the A (B) sub-lattice. The black dashed arrows indicate the manner of spin precessions associated with the left-handed magnon mode, where $\boldsymbol{S}_A$ has a larger amplitude than $\boldsymbol{S}_B$. On the contrary, the right-handed mode is characterized by a larger precession of $\boldsymbol{S}_B$ over $\boldsymbol{S}_A$ (not shown). (b) and (c) depict the two distinct ways of connecting the ribbon into a Möbius strip. While the AFM ground state is compatible with the TBC, the excited states in the form of circularly-polarized magnons are radically disrupted.

As illustrated in Fig. 1(a), we consider a nano-ribbon composed of two ferromagnetic spin chains oppositely aligned, forming an effective antiferromagnetic (AFM) system involving two sub-lattices. The nano-ribbon can be wrapped into a Möbius strip using two distinct ways of twisting based on Fig. 1(b) and (c). To motivate the following discussions, we first make a critical observation: although the ground-state AFM spin configuration is compatible with the Möbius TBC, the magnons excitations with circular polarizations are inherently irreconcilable with the system topology. Specifically, when only the exchange interactions and the easy-axis anisotropy are considered, the system respects the $O(2)$ rotational symmetry in the spin space. Consequently, the magnon eigenmodes disregarding the TBC are circularly polarized, exhibiting either left-handed or right-handed chirality for both spin species [18–20]. For example, in the left-handed mode, $\boldsymbol{S}_A$ and $\boldsymbol{S}_B$ both rotate clockwisely, but $\boldsymbol{S}_A$ has a larger oscillation amplitude, which is indicated by the black dashed arrows. As illustrated in Fig. 1(b) and (c), however, imposing the Möbius TBC by connecting the 1 and N sites with A and B swapped will inevitably disrupt both the chirality and the amplitude of the spin precessions. Therefore, the magnon solutions that are commensurate with the Möbius topology must be fundamentally different from the circularly-polarized magnons widely known for collinear AFM materials.

Model and Results. Let us start with the AFM spin configuration depicted in Fig. 1(a), where the red and blue arrows indicate the spins on the A and B sub-lattices for the ground state. A Möbius strip can then be constructed based on either Fig. 1(b) or Fig. 1(c), which are topologically distinct and satisfy different TBCs to be specified later. Excluding any geometric effects originating from the curvature of the strip [21–26], we consider a minimal Hamiltonian that preserves the local rotational symmetry about the local z axis:

$$\begin{aligned} H_0 = &- J_F \sum\nolimits_{\langle i,j\rangle} (\boldsymbol{S}_{Ai}\cdot\boldsymbol{S}_{Aj} + \boldsymbol{S}_{Bi}\cdot\boldsymbol{S}_{Bj}) \\ &+ J_{AF}\sum\nolimits_i \boldsymbol{S}_{Ai}\cdot\boldsymbol{S}_{Bi} - K\sum\nolimits_i ({S^z_{Ai}}^2 + {S^z_{Bi}}^2), \end{aligned} \tag{1}$$

where i labels the lattice on the strip, J_F (J_{AF}) is the nearest-neighbor exchange interaction for (between) the same (different) spin species, and K is the perpendicular easy-axis anisotropy. In our convention, all these parameters are positive. Contrary to a single ferromagnet spin chain arranged on a Möbius strip [23, 27], our system is free from geometrical frustration, thus no domain walls are present in the ground state.

To derive the quantum magnon excitations, we apply the linearized Holstein–Primakoff transformations on the spin raising and lowering operators, $S^{\pm} = S_x \pm \mathrm{i}S_y$, for each sublattice

$$S^+_{Ai} \approx \sqrt{2S}a_i, \quad S^-_{Ai} \approx \sqrt{2S}a^\dagger_i, \quad S^z_{Ai} = S - a^\dagger_i a_i, \tag{2a}$$
$$S^+_{Bi} \approx \sqrt{2S}b^\dagger_i, \quad S^-_{Bi} \approx \sqrt{2S}b_i, \quad S^z_{Bi} = b^\dagger_i b_i - S, \tag{2b}$$

where a_i (b_i) represents the annihilation of a magnon on site i and sublattice A (B), and S is the spin magnitude on each site. By neglecting the constant terms, we obtain the magnon Hamiltonian as

$$\begin{aligned} H =&(2K + 2J_F + J_{AF})S\sum\nolimits_i (a^\dagger_i a_i + b^\dagger_i b_i) \\ &- J_F S\sum\nolimits_{\langle i,j\rangle} (a^\dagger_i a_j + a^\dagger_j a_i + b^\dagger_i b_j + b^\dagger_j b_i) \\ &+ J_{AF}S\sum\nolimits_i (a^\dagger_i b^\dagger_i + a_i b_i). \end{aligned} \tag{3}$$

We cannot directly apply Fourier transformations to Eq. (3) because the PBCs, $a_{i+N} = a_i$ and $b_{i+N} = b_i$, are explicitly broken. Instead, we have

$$a_{i+N} = b_i, \qquad b_{i+N} = a_i, \tag{4}$$

which means the definitions of A and B chains are interchanged after winding around the Möbius strip by 2π. Regarding Eq. (4), we recombine a_i and b_i to define the following operators:

$$\alpha_i = \frac{1}{\sqrt{2}}(a_i - b_i)e^{\mathrm{i}\xi\frac{\pi x_i}{L}}, \qquad \beta_i = \frac{1}{\sqrt{2}}(a_i + b_i), \tag{5}$$

where x_i specifies the position of site i from 1 to N along the strip [see Fig. 1], L is the total length of the nanoribbon, and $\xi = \pm 1$ corresponds the two distinct ways of connection illustrated in Fig. 1(b) and 1(c). The new magnon operators α_i and β_i satisfy not only the bosonic commutation relations but also the PBCs: $\alpha_{i+N} = \alpha_i$ and $\beta_{i+N} = \beta_i$. Using this new set of basis, the magnon Hamiltonian Eq. (3) becomes

$$\begin{aligned} H =&(2K + 2J_F + J_{AF})S\sum\nolimits_i \left[\alpha^\dagger_i\alpha_i + \beta^\dagger_i\beta_i\right] \\ &- J_F S\sum\nolimits_{\langle i,j\rangle}\left[e^{\mathrm{i}\pi\xi(x_i - x_j)/L}\alpha^\dagger_i\alpha_j + \beta^\dagger_i\beta_j + h.c.\right] \\ &- \frac{J_{AF}S}{2}\sum\nolimits_i \left[e^{\mathrm{i}2\pi\xi x_i/L}\alpha^\dagger_i\alpha^\dagger_i - \beta^\dagger_i\beta^\dagger_i + h.c.\right], \end{aligned} \tag{6}$$

where $h.c.$ denotes hermitian conjugate. Equation (6) is naturally decomposed into $H = H_\alpha + H_\beta$ for the α_i and β_i sectors. Applying the Fourier transformations

$$\alpha_k = \frac{1}{\sqrt{2N}}\sum\nolimits_i e^{-\mathrm{i}(k - \xi\pi/L)x_i}(a_i - b_i), \tag{7a}$$
$$\beta_k = \frac{1}{\sqrt{2N}}\sum\nolimits_i e^{-\mathrm{i}kx_i}(a_i + b_i), \tag{7b}$$

we can derive the momentum-space Hamiltonian. To this end, we adopt the Bogoliubov-de-Gennes (BdG) basis

$$\Psi_\alpha = (\alpha_k,\, \alpha^\dagger_{-k+2\pi\xi/L})^{\mathrm{T}}, \quad \Psi_\beta = (\beta_k,\, \beta^\dagger_{-k})^{\mathrm{T}} \tag{8}$$

with $l = L/N$ being the lattice constant, $H_\alpha = \Psi^\dagger_\alpha\mathcal{H}_\alpha\Psi_\alpha$ and $H_\beta = \Psi^\dagger_\beta\mathcal{H}_\beta\Psi_\beta$. Here, the BdG Hamiltonian reads

$$\mathcal{H}_{\alpha(\beta)} = S\begin{pmatrix} Q_{\alpha(\beta)} & -J_{AF}/2 \\ -J_{AF}/2 & Q_{\alpha(\beta)} \end{pmatrix}, \tag{9}$$

where $Q_\alpha = K + J_{AF}/2 + J_F[1 - \cos{(k - \xi\pi/L)l}]$ and $Q_\beta = K + J_{AF}/2 + J_F[1 - \cos{(kl)}]$. It should be noted that in the α sector, magnons of momentum k couple those of momentum $-k + 2\pi\xi/L$; whereas in the β sector, k pairs with $-k$ without a shift.

Owing to the bosonic commutation relations of the BdG basis, we need to diagonalize $\sigma_z\mathcal{H}_{\alpha(\beta)}$ rather than $\mathcal{H}_{\alpha(\beta)}$ for the magnon solutions [28]. In this regard, we obtain the eigen-frequencies (we set $\hbar = 1$)

$$\omega^{\pm}_{\alpha(\beta)} = \pm S\sqrt{q^1_{\alpha(\beta)}q^2_{\alpha(\beta)}} \tag{10}$$

with the corresponding eigenvectors

$$v^{\pm}_{\alpha(\beta)} = \left(\sqrt{q^1_{\alpha(\beta)}} \pm \sqrt{q^2_{\alpha(\beta)}}, \sqrt{q^1_{\alpha(\beta)}} \mp \sqrt{q^2_{\alpha(\beta)}}\right)^{\mathrm{T}} \tag{11}$$

where $q^1_{\alpha(\beta)} = Q_{\alpha(\beta)} + J_{AF}/2$ and $q^2_{\alpha(\beta)} = Q_{\alpha(\beta)} - J_{AF}/2$ are both positive. The negative frequency branches and their associated eigenvectors are redundant solutions, which can be interpreted as a *hole* representation. For instance, $v^-_\beta(k)$ describes a hole at k that corresponds to a real β-magnon at $-k$. A similar picture is applicable to the α branch so long as the $2\pi\xi/L$ momentum shift appearing in Eq. (8) is taken into account. Consequently, $v^+_{\alpha(\beta)}$ and $v^-_{\alpha(\beta)}$ are linearly dependent, representing one unique physical solution.

Let us concentrate on the positive frequency branches and consider the $\xi = 1$ connection [*i.e.*, Fig. 1(b)]. For simplicity, we also omit the super-index $+$. With a proper normalization of $v^+_{\alpha(\beta)}$, the magnon eigenmodes associated with $\omega_{\alpha(\beta)}$ are described by

$$\tilde{\alpha}_k = \frac{\sqrt{q^1_\alpha} + \sqrt{q^2_\alpha}}{2\sqrt{Q_\alpha}}\alpha_k + \frac{\sqrt{q^1_\alpha} - \sqrt{q^2_\alpha}}{2\sqrt{Q_\alpha}}\alpha^\dagger_{-k+2\pi/L} \tag{12a}$$

$$\tilde{\beta}_k = \frac{\sqrt{q^1_\beta} + \sqrt{q^2_\beta}}{2\sqrt{Q_\beta}}\beta_k + \frac{\sqrt{q^1_\beta} - \sqrt{q^2_\beta}}{2\sqrt{Q_\beta}}\beta^\dagger_{-k} \tag{12b}$$

and their $\tilde{\alpha}^\dagger_k$, $\tilde{\beta}^\dagger_k$ counterparts. Figure 2(a) and (b) plot the discretized dispersion relations for $N = 10$ (only the lowest few states on each branch are shown), along with illustrations of the magnon eigenmodes at $k = 0$. While the β modes distribute symmetrically $\omega_\beta(-k) = \omega_\beta(k)$, the α branch shifts rightward by $\delta k = \pi/L$ such that $\omega_\alpha(-k) = \omega_\alpha(k + 2\delta k)$. The skewed $\omega_\alpha(k)$ is intimately related to the asymmetric paring of Ψ_α in Eq. (8), which originates from the non-trivial topology of the Möbius strip. It is easy to verify that setting $\xi = -1$ [*i.e.*, using the connection of Fig. 1(c)] leads to a leftward shift of $\omega_\alpha(k)$, or $\delta k = -\pi/L$. Interestingly, if we reversely count the sites on the strip, the spectral shift δk also flips sign, but in this case the eigenvectors are different from what one would obtain for $\xi = -1$.

To better understand the magnon eigenmodes, we now express Eq. (12) in terms of the original spin variables. Using $S^\pm = S^x \pm \mathrm{i}S^y$ and Eqs. (2) and (7), we obtain

$$\tilde{\alpha}^\dagger_k = \sum_i \frac{e^{\mathrm{i}(k-\delta k)x_i}}{2\sqrt{NSQ_\alpha}}\left[\sqrt{q^1_\alpha}S^x_{Ai} - \mathrm{i}\sqrt{q^2_\alpha}S^y_{Ai} - \sqrt{q^1_\alpha}S^x_{Bi} - \mathrm{i}\sqrt{q^2_\alpha}S^y_{Bi}\right], \tag{13a}$$

$$\tilde{\beta}^\dagger_k = \sum_i \frac{e^{\mathrm{i}kx_i}}{2\sqrt{NSQ_\beta}}\left[\sqrt{q^1_\beta}S^x_{Ai} - \mathrm{i}\sqrt{q^2_\beta}S^y_{Ai} + \sqrt{q^1_\beta}S^x_{Bi} + \mathrm{i}\sqrt{q^2_\beta}S^y_{Bi}\right], \tag{13b}$$

where it is important to note that $q^1_{\alpha(\beta)} > q^2_{\alpha(\beta)} > 0$. In the classical limit, both the α and β branches feature a right-handed (left-handed) elliptical precession of

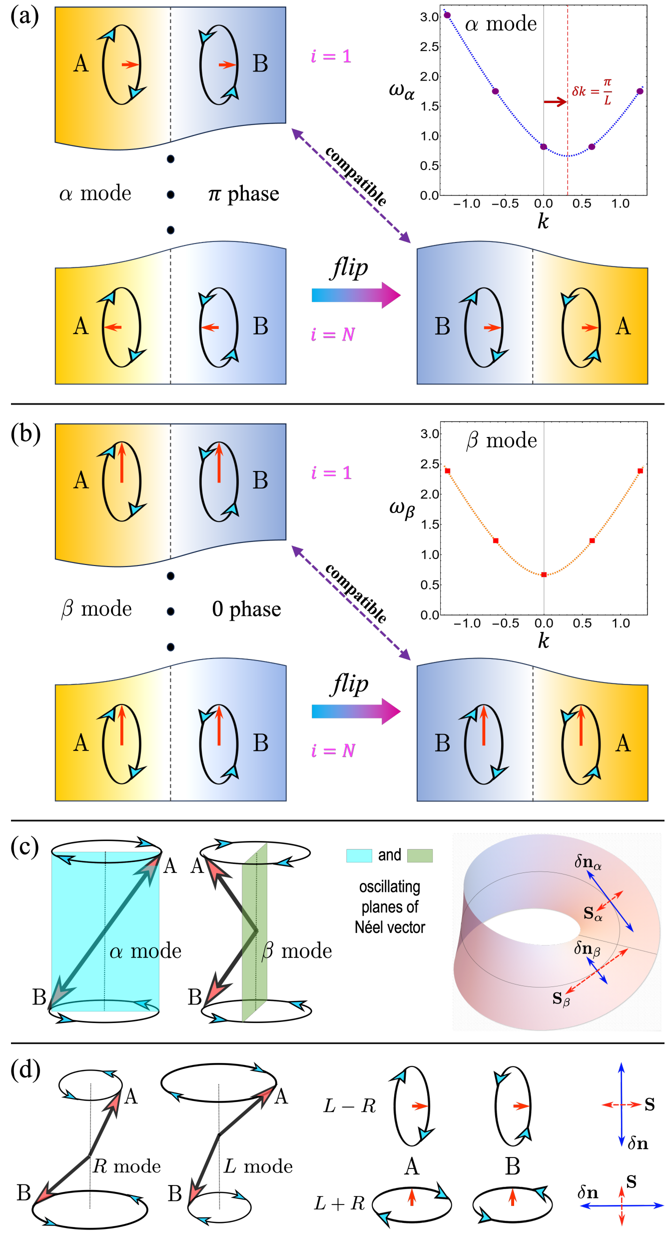

FIG. 2. (a, b) Illustrations of the α and β modes at $k = 0$, and the plots of the lowest few modes on each branch for $\xi = 1$, $N = 10$, $l = 1$, $S = 2$, $J_F = J_{AF} = 1$, and $K = 0.1$. While $\omega_\beta(-k) = \omega_\beta(k)$ is symmetric, $\omega_\alpha(-k) = \omega_\alpha(k + 2\delta k)$ is skewed by $\delta k = \pi/L$. The spectral shift of the α branch is accompanied by an intrinsic π phase difference in the spin precessions between sites $i = 1$ and $i = N$, reflecting the impact of the Möbius TBC. (c) Left: a 3D illustration of the spin precessions in the α and β modes, where $\boldsymbol{S}_A$ and $\boldsymbol{S}_B$ rotate elliptically with an equal amplitude and opposite chirality, rendering the Néel vector linearly-polarized (see the color-shaded planes). Right: an illustration of the oscillating Néel vector (solid blue) and the oscillating spin vector (dashed red) for the α and β modes based on Eq. (15). That $\delta\boldsymbol{n}_\alpha \perp \delta\boldsymbol{n}_\beta$ should not be confused by their being shown in different locations. (d) Ordinary right-circular (R) and left-circular (L) magnon modes, and their superposition $L - R$ and $L + R$ characterized by a linearly-polarized Néel vector (solid blue) orthogonal to the oscillating spin vector (dashed red).

$\boldsymbol{S}_A$ ($\boldsymbol{S}_B$) with the major axes lying in the x direction; $\boldsymbol{S}_A$ and $\boldsymbol{S}_B$ always precess about the easy-axis with the same amplitude and opposite chirality. The distinctions between the two branches manifest in two aspects, as schematically demonstrated in Fig. 2(a)–(c). First, from a local bird-eye view, $\boldsymbol{S}_A$ and $\boldsymbol{S}_B$ in the α-mode at $k = 0$ overlap with each other when passing the minor axes of their elliptical trajectories while becoming back-to-back when passing the major axes. On the contrary, $\boldsymbol{S}_A$ and $\boldsymbol{S}_B$ in the β-mode at $k = 0$ are back-to-back on the minor axes while overlapping each other on the major axes. Second, due to the momentum shift $\delta k = \pi/L$ in the α branch, the spin precessions on site $i = N$ differ from those on site $i = 1$ by a π phase even for $k = 0$, which exactly compensates the impact of the Möbius TBC that connects sites 1 and N with a flip. In contrast, the β mode at $k = 0$ does not exhibit a phase difference between $i = 1$ and $i = N$, which, in combination with the first distinction above, is just commensurate with the Möbius TBC.

Discussion. To demonstrate the unique characteristics of the magnon eigenmodes, we draw a 3D perspective in Fig. 2(c) where $\boldsymbol{S}_A$ and $\boldsymbol{S}_B$ share the same origin such that their precessional trajectories are concentric about the local z axis. It is easy to deduce that the Néel vector $\boldsymbol{n} = (\boldsymbol{S}_A - \boldsymbol{S}_B)/2S$ undergoes a pendulum-like oscillation restricted to the plane containing the major (minor) axes of the two elliptical trajectories in an α mode (β mode). Comparatively, the total spin vector $\boldsymbol{S} = (\boldsymbol{S}_A + \boldsymbol{S}_B)/2S$ oscillates linearly on a plane orthogonal to that of the Néel vector. That is to say, by the standard of spin wave polarization [19, 20], both the α and β modes are linearly polarized, thus being devoid of chirality.

The above intuitive picture can be corroborated by a straightforward algebra. According to Eqs. (12) and (13), the real-time evolution of the classical spin vectors is

$$\boldsymbol{S}^{\alpha}_{A/B} \sim \mathrm{Re}\Big[\Big(\pm\sqrt{q^1_\alpha}\hat{x} + \mathrm{i}\sqrt{q^2_\alpha}\hat{y}\Big)\, e^{\mathrm{i}\omega_\alpha t - \mathrm{i}(k-\delta k)x}\Big], \quad (14a)$$

$$\boldsymbol{S}^{\beta}_{A/B} \sim \mathrm{Re}\Big[\Big(\sqrt{q^1_\beta}\hat{x} \pm \mathrm{i}\sqrt{q^2_\beta}\hat{y}\Big)\, e^{\mathrm{i}(\omega_\beta t - kx)}\Big], \quad (14b)$$

for the α- and β-branch, respectively, where the + (−) sign corresponds to the A (B) sublattice. From Eq. (14), we can read off the oscillating components of the Néel vector and the total spin vector as

$$\delta\boldsymbol{n}_\alpha(k) \sim \hat{x}\sqrt{q^1_\alpha}\cos\left[\omega_\alpha(k)t - (k-\delta k)\,x\right], \quad (15a)$$

$$\boldsymbol{S}_\alpha(k) \sim \hat{y}\sqrt{q^2_\alpha}\sin\left[\omega_\alpha(k)t - (k-\delta k)\,x\right], \quad (15b)$$

$$\delta\boldsymbol{n}_\beta(k) \sim \hat{y}\sqrt{q^2_\beta}\sin\left[\omega_\beta(k)t - kx\right], \quad (15c)$$

$$\boldsymbol{S}_\beta(k) \sim \hat{x}\sqrt{q^1_\beta}\cos\left[\omega_\beta(k)t - kx\right], \quad (15d)$$

all of which are indeed linearly polarized bearing null chirality, confirming the picture inferred in Fig. 2(c). As $q^1_{\alpha(\beta)} > q^2_{\alpha(\beta)} > 0$, the oscillation amplitude of the Néel vector is larger (smaller) than that of the total spin in an α (β) mode, namely, $|\delta\boldsymbol{n}_\alpha| > |\boldsymbol{S}_\alpha|$ and $|\delta\boldsymbol{n}_\beta| < |\boldsymbol{S}_\beta|$. The geometry embedded in Eq. (15) is illustrated by the right panel of Fig. 2(c).

Since the total number of sites $N = L/l$ is finite, the magnon eignmodes must be discrete, taking place only at $k = 0, \pm 2\pi/L, \pm 4\pi/L\ \cdots$ as plotted in Fig. 2. Because the spectrum $\omega_\alpha(k) \neq \omega_\alpha(-k)$ is skewed by $\delta k = \pi/L$ while $\omega_\beta(k) = \omega_\beta(-k)$ is symmetric, only the β modes can form standing waves on the Möbius strip, whereas the α modes cannot. Consider the Néel vector for example, $\delta\boldsymbol{n}_\beta(k) + \delta\boldsymbol{n}_\beta(-k) \sim \hat{y}\sin\omega_\beta t\cos kx$, where t and x are separated, hence representing a standing wave. For the α branch, $\omega_\alpha(-k) = \omega_\alpha(k + 2\delta k)$, thus time and space do not separate in $\delta\boldsymbol{n}_\alpha(k) + \delta\boldsymbol{n}_\alpha(-k)$, prohibiting the formation of standing waves. The disparity between the α and β branches is an intrinsic topological property of the AFM magnons on a Möbius strip.

At this point, it is instructive to compare the unique magnon eigenmodes on a Möbius strip with what would become the eigenmodes if the nano-ribbon in Fig. 1(a) is wrapped into a topologically trivial band without twisting (which imposes an ordinary PBC). The latter case only admits the well-known eigenmodes in collinear AFM materials [29] because we have excluded the local curvature effect in our model. To this end, Fig. 2(d) illustrates the right-circular (R) and left-circular (L) eignmodes, as well as their coherent superposition $L - R$ and $L + R$ featuring elliptical precessions of $\boldsymbol{S}_A$ and $\boldsymbol{S}_B$ with opposite chirality, which leads to a linearly-polarized oscillation of the Néel vector $\boldsymbol{n}$ without chirality (so does the total spin vector $\boldsymbol{S}$). While $L - R$ is locally identical to the α mode shown in Fig. 2(a), it is not accompanied by a built-in π phase shift at $k = 0$, let alone a spectral shift. The β modes are not even locally similar to $L - R$ or $L + R$, which are emergent eigenmodes enabled by the Möbius topology. Unlike $L - R$ and $L + R$, neither α nor β can be expressed as linear superposition of R and L. This is because a Möbius strip is a non-orientable manifold on which the chirality of spin precessions becomes ambiguous globally, given that $+z$ and $-z$ are indistinguishable. In other words, the eigenspace spanned by α and β is not smoothly connected to that spanned by R and L; they belong to distinct topological classes.

It is established that in easy-axis AFM materials such as MnF_2 [19, 30], R and L are degenerate in energy in the absence of magnetic fields. In easy-plane AFM materials such as NiO, the existence of hard-axis anisotropy breaks the rotational symmetry and lifts the degeneracy, rendering $L - R$ and $L + R$ the magnon eigenmodes [20, 29]. That is to say, symmetry dictates the nature of eigenmodes. The spin Hamiltonian we adopted in this Letter, however, preserves the local rotational symmetry (with respect to the local easy axis). Therefore, the suppression of the circularly-polarized modes, hence the absence of chirality in the Néel vector dynamics, is solely attributed to the Möbius topology. This introduces an intriguing but hitherto unknown mechanism: Non-trivial topology in the real space alone can lead to spontaneous symmetry breaking in the eigenspace of elementary excitations without the aid of symmetry-breaking interactions. The physical consequence manifests as a lifted degeneracy of the eigenmodes which possess a lower symmetry than the Hamiltonian. Because a quantum of angular momentum associated with the R-(L-)circular mode is $+\hbar$ ($-\hbar$), the TISB we found here is followed by the suppression of longitudinal magnon spin currents on a Möbius strip.

To close our discussion, we mention that the lowest β mode ($k = 0$) is in principle observable via the AFM resonance driven by a microwave, while the α modes are difficult to probe as they are at odds with standing waves. Nonetheless, our findings are amenable to meta-materials such as magnonic crystals, wherein an α-mode locally excited by an oscillating magnetic field will propagate in opposite directions but can never form standing waves, leaving a non-reciprocal circulation of energy along the strip which is detectable by optical methods.

Outlook. Even though we have demonstrated the TISB in the AFM magnons on a Möbius strip, the mechanism itself is general and can manifest in other contexts with different quasiparticles or TBCs. For example, we anticipate that the eigenmodes of phonon excitations on a Möbius strip to be linearly polarized while the circularly-polarized chiral phonons are suppressed by the Möbius topology. For photons that are governed by Maxwell's equations, the axis of circular polarization is parallel to the momentum $\boldsymbol{k}$, which defines a distinct geometry compared to ours, calling for a separate investigation. For tight-binding electrons on a Möbius strip, while the Hamiltonian is very similar to ours, the fermionic statistics brings a fundamental distinction in the diagonalization [which does not involve σ_z as that in Eq. (10)]. Under alternative TBCs such as a Klein bottle, even the AFM magnons could acquire new features of TISB beyond what we showed in this Letter. Therefore, our findings could greatly inspire a broader research endeavor in the near future highlighting the profound impact of real-space topology on the physical nature of elementary excitations.

We thank Qian Niu for helpful discussions. This work is supported by the Air Force Office of Scientific Research under Grant No. FA9550-19-1-0307.

---

* kuangyid@ucr.edu
† rancheng@ucr.edu

[1] B. A. Bernevig, *Topological Insulators and Topological Superconductors* (Princeton University Press, Princeton, 2013).
[2] Z.-L. Guo, Z. Gong, H. Dong, and C. Sun, Möbius graphene strip as a topological insulator, Physical Review B **80**, 195310 (2009).
[3] L.-T. Huang and D.-H. Lee, Topological insulators on a mobius strip, Physical Review B **84**, 193106 (2011).
[4] X. Wang, X. Zheng, M. Ni, L. Zou, and Z. Zeng, Theoretical investigation of möbius strips formed from graphene, Applied Physics Letters **97**, 123103 (2010).
[5] E. W. Caetano, V. N. Freire, S. Dos Santos, D. S. Galvao, and F. Sato, Möbius and twisted graphene nanoribbons: Stability, geometry, and electronic properties, The Journal of chemical physics **128**, 164719 (2008).
[6] Y. Liu, L.-R. Ding, A.-L. He, and Y.-F. Wang, Quantum transport in Chern insulators on Möbius strips, Journal of Physics: Condensed Matter **32**, 505501 (2020).
[7] L. N. Monteiro, C. A. S. Almeida, and J. E. G. Silva, Dirac fermions on wires confined to the graphene möbius strip, Phys. Rev. B **108**, 115436 (2023).
[8] K. Flouris, M. M. Jimenez, and H. J. Herrmann, Curvature-induced quantum spin-hall effect on a möbius strip, Phys. Rev. B **105**, 235122 (2022).
[9] N. Nishiguchi and M. N. Wybourne, Phonon modes in a möbius band, Journal of Physics Communications **2**, 085002 (2018).
[10] D. M. Walba, R. M. Richards, and R. C. Haltiwanger, Total synthesis of the first molecular möbius strip, Journal of the American Chemical Society **104**, 3219 (1982).
[11] G. Ouyang, L. Ji, Y. Jiang, F. Würthner, and M. Liu, Self-assembled möbius strips with controlled helicity, Nature Communications **11**, 5910 (2020).
[12] S. Tanda, T. Tsuneta, Y. Okajima, K. Inagaki, K. Yamaya, and N. Hatakenaka, A möbius strip of single crystals, Nature **417**, 397 (2002).
[13] D. J. Ballon and H. U. Voss, Classical möbius-ring resonators exhibit fermion-boson rotational symmetry, Phys. Rev. Lett. **101**, 247701 (2008).
[14] X.-B. Xu, L. Shi, G.-C. Guo, C.-H. Dong, and C.-L. Zou, "möbius" microring resonator, Applied Physics Letters **114** (2019).
[15] Y. Chen, J. Hou, G. Zhao, X. Chen, and W. Wan, Topological resonances in a möbius ring resonator, Communications Physics **6**, 84 (2023).
[16] T. Bauer, P. Banzer, E. Karimi, S. Orlov, A. Rubano, L. Marrucci, E. Santamato, R. W. Boyd, and G. Leuchs, Observation of optical polarization möbius strips, Science **347**, 964 (2015).
[17] J. Kreismann and M. Hentschel, The optical möbius strip cavity: Tailoring geometric phases and far fields, Europhysics Letters **121**, 24001 (2018).
[18] Y. Yafet and C. Kittel, Antiferromagnetic arrangements in ferrites, Phys. Rev. **87**, 290 (1952).
[19] F. Keffer and C. Kittel, Theory of antiferromagnetic resonance, Phys. Rev. **85**, 329 (1952).
[20] R. Cheng, M. W. Daniels, J.-G. Zhu, and D. Xiao, Antiferromagnetic spin wave field-effect transistor, Scientific reports **6**, 24223 (2016).
[21] D. D. Sheka, V. P. Kravchuk, and Y. Gaididei, Curvature effects in statics and dynamics of low dimensional magnets, Journal of Physics A: Mathematical and Theoretical **48**, 125202 (2015).
[22] D. D. Sheka, O. V. Pylypovskyi, O. M. Volkov, K. V. Yershov, V. P. Kravchuk, and D. Makarov, Fundamentals of curvilinear ferromagnetism: statics and dynamics of geometrically curved wires and narrow ribbons, Small **18**, 2105219 (2022).
[23] M. Yoneya, K. Kuboki, and M. Hayashi, Domain-wall

structure of a classical heisenberg ferromagnet on a möbius strip, Physical Review B **78**, 064419 (2008).

[24] L. Körber, *Spin waves in curved magnetic shells*, Ph.D. thesis (2023).

[25] A. Fernández-Pacheco, R. Streubel, O. Fruchart, R. Hertel, P. Fischer, and R. P. Cowburn, Three-dimensional nanomagnetism, Nature communications **8**, 15756 (2017).

[26] R. Streubel, P. Fischer, F. Kronast, V. P. Kravchuk, D. D. Sheka, Y. Gaididei, O. G. Schmidt, and D. Makarov, Magnetism in curved geometries, Journal of Physics D: Applied Physics **49**, 363001 (2016).

[27] O. V. Pylypovskyi, V. P. Kravchuk, D. D. Sheka, D. Makarov, O. G. Schmidt, and Y. Gaididei, Coupling of chiralities in spin and physical spaces: the möbius ring as a case study, Physical Review Letters **114**, 197204 (2015).

[28] W. Nolting and A. Ramakanth, *Quantum Theory of Magnetism* (Springer-Verlag, New York, 2009).

[29] S. M. Rezende, A. Azevedo, and R. L. Rodríguez-Suárez, Introduction to antiferromagnetic magnons, Journal of Applied Physics **126** (2019).

[30] P. Vaidya, S. A. Morley, J. van Tol, Y. Liu, R. Cheng, A. Brataas, D. Lederman, and E. Del Barco, Subterahertz spin pumping from an insulating antiferromagnet, Science **368**, 160 (2020).